Research Square

Preprints are preliminary reports that have not undergone peer review.
They should not be considered conclusive, used to inform clinical practice,
or referenced by the media as validated information.

Comparative Electrothermal Performance Analysis of Three-Phase and Six-Phase Induction Motors for Electric Vehicle Applications Under HWFET, WLTP and Urban Drive Cycles Using ANSYS Motor-CAD: A Sustainable Traction Approach

Asuquo Eke

ekeasuquo@gmail.com

Cross River State University of Technology: Cross River University of Technology
https://orcid.org/0009-0000-9576-2910

Research Article

Keywords: Six-phase induction motor, Three-phase induction motor, Electrothermal analysis, Electric vehicle traction, ANSYS Motor-CAD

Posted Date: November 26th, 2026

DOI: https://doi.org/10.21203/rs.3.rs-11862064/v1

License: This work is licensed under a Creative Commons Attribution 4.0 International License.
Read Full License

Additional Declarations: The authors declare no competing interests.

Comparative Electrothermal Performance Analysis of Three-Phase and Six-Phase Induction Motors for Electric Vehicle Applications Under HWFET, WLTP and Urban Drive Cycles Using ANSYS Motor-CAD: A Sustainable Traction Approach.

Asuquo Eke[1], Ake, David[2], Ohiero Peter, O.I. Okoro[2], A. J. Onah[3], E.J. Akpama[4]

Department of Electrical/Electronic Engineering, Cross River University of Technology, Calabar. Nigeria
Department of Electrical/Electronic Engineering Admiralty University of Nigeria, Delta State. Nigeria
Department of Electrical/Electronic Engineering, Cross River University of Technology, Calabar. Nigeria
Department of Electrical and Electronic Engineering, Michael Okpara University of Agriculture, Umudike. Abia State. Nigeria
Department of Electrical and Electronic Engineering, Michael Okpara University of Agriculture, Umudike. Abia State. ***Nigeria***
Department of Electrical/Electronic Engineering, Cross River University of Technology, Calabar. Nigeria

***** Correspondence: ekeasuquo@gmail.com, (+234-7039102495)

Corresponding author, **Asuquo Eke[1]:** *Cross River University of Technology, Calabar. Nigeria*

ABSTRACT

This study involves the comparative analysis of the electrothermal performance of a three-phase and a six-phase squirrel-cage induction motor in an electric vehicle (EV) traction application. The purpose of this paper is to meet the need for economical, thermally stable, reliable, and environmentally acceptable electric drives. The two induction motors under consideration have the same rating; the power is 1.5kW, voltage is 380V, frequency is 50Hz, number of poles is 4, and the rated speed is approximately 1450rpm. The electrothermal performance of the two motors was predicted using ANSYS Motor-CAD. A combined electromagnetic-thermal model was used to evaluate losses, efficiency, temperature rise, torque, and energy consumption during the drive cycle. The hardware-in-loop tests were carried out to verify the simulation results. The same vehicle parameters, traction torque requirements as well as cooling conditions and operational constraints were taken into account for the two motor drives under investigation in order to ensure a fair comparative analysis. It is found that the six-phase induction motor has a better electrothermal performance than its three-phase counterpart. Average efficiency values of 91.4%, 90.1%, and 87.3% were recorded for a six-phase induction motor drive during HWFET, WLTP, and urban driving, respectively. The corresponding values for a three-phase induction motor were 88.7%, 86.9%, and 82.8%, respectively. As a result, the maximum stator temperature was reduced from 91.8oC to 82.6oC, 104.7oC to 93.1oC, and 118.6oC to 101.4oC for HWFET, WLTP, and urban driving cycles. Moreover, the energy losses for the six-phase induction motor were 16.3%, 16.5%, and 18.7% lower than those of the three-phase induction motor for the same driving cycles. Therefore, the paper concludes that a six-phase induction motor is more efficient, reliable, and eco-friendly.

Keywords: Six-phase induction motor; Three-phase induction motor; Electrothermal analysis; Electric vehicle traction; ANSYS Motor-CAD.

1.0 Introduction

A promising way to reduce transportation energy use, greenhouse gas emissions, and oil consumption is the transition from conventional internal combustion vehicles to electric vehicles (EVs). Research on electric propulsion devices with high efficiency, high torque density, wide operating speed ranges, high reliability, and long operating life has been advanced to meet the increased interest in EVs. The properties of the traction motor in an EV propulsion system are of great importance since they influence the vehicle's acceleration capabilities, cruising performance, regeneration efficiency, range, energy consumption, reliability, and environmental friendliness. The thermal characteristics of the traction motor have become a limiting factor in the design of EV propulsion systems due to the need for improved power density. Electric motors for vehicle propulsion operate under the diverse operating conditions of acceleration, deceleration, regenerative braking, cruising, launch, hills climbing, and stop-and-go process, contrary to industrial motors. The motor experiences varying levels of heating as a result of the variations in speed, torque, current, slip, and losses that occur throughout these events. The sequence and length of the operating conditions dictated by the particular driving cycle of the vehicle affect the thermal characteristics of the motor as well as the defined operating conditions. According to recent studies, different driving cycles may cause different motor thermal responses owing to differences in acceleration, deceleration, speed, and load profiles. As a result of the conversion of the waste energy from the motor into heat, it is critical that appropriate thermal management be used in EVs in order to get the right mix of power density, efficiency, lifetime, and dependability. Stator copper losses, rotor copper losses, iron or core losses, mechanical losses, and stray-load losses are all sources of heat in an induction motor. Operating temperature, machine design, slip, magnetic flux density, speed, frequency, and current are all factors that contribute to the generation of heat. High temperatures have the potential to cause insulation degradation, mechanical stress, lower efficiency, and a shorter service life by increasing the winding resistance, which leads to higher copper losses and hence more heat production. Effective thermal management is critical for withstanding the heat generated, maintaining the motor's performance, and extending its life, according to recent assessments of EV motor technologies. The importance of

taking into account motor power ratings, heat generation, and dissipation in connection to the motor's size and weight limits is highlighted by the investigation of air, liquid, hybrid, and novel cooling techniques. They are also attractive in difficult traction situations due to their sturdy build. However, the rotor copper losses that are characteristic of induction machines can become considerable during high-slip and high-torque operational situations. Thus, the thermal characteristics of the rotor and stator need to be meticulously assessed when designing an induction motor for electric vehicle propulsion (Wang et al., 2022; Prasanna et al., 2026). Whereas the traditional three-phase setup is not the only architecture for EV propulsion using induction machines. Because of their potential advantages in torque generation, fault tolerance, power distribution, dependability, and thermal efficiency, six-phase induction motors a form of multiphase electric machine are attracting more and more attention from researchers. A six-phase machine adds extra stator phases and degrees of freedom to the drive system. By distributing the electrical load among several phases, this configuration helps reduce the current in each phase and change copper losses and heat generation. Multiphase architectures can also offer redundancy, enabling the machine to maintain operation on specific phase or inverter faults, which is especially important in safety-critical transportation contexts (El Baghdadi & Hegazy, 2023). Recent literature has increasingly acknowledged the potential of multiphase machines for transportation. El Baghdadi and Hegazy (2023) examined multiphase motors and drive systems in EV powertrains, highlighting fault tolerance, enhanced reliability, improved power density, and adaptable control as key reasons for the adoption of the multiphase technology. The examination also highlighted the fact that multiphase machines can be combined with sophisticated power-electronic converters. In particular, thermal characteristics have emerged as a significant factor for evaluating multiphase induction motors. Priyanka et al. (2022) examined the thermal properties of multiphase induction motors for electric vehicle applications, focusing on heat production and release within the device. Their research is particularly pertinent to the current study as they highlighted the necessity of analyzing the thermal behavior of multiphase induction machines instead of assessing their performance from an electromagnetic and control standpoint only. The study provides an essential foundation for investigating whether distributing electrical demand over different phases might improve the thermal setting in EV traction scenarios. The development of six-phase induction motors for electric vehicle propulsion has been demonstrated by recent studies. Abdelwanis (2025) used fuzzy-PID control, space-vector modulation, and direct torque control to study an EV drive based on a six-phase induction motor. The study concluded that the six-phase configuration has the potential to be a suitable solution for modern EV propulsion systems because it enhanced dynamic speed tracking and decreased current and voltage harmonic distortions. Moreover, the modified multiphase induction motor was compared to the conventional three-phase induction motor by the researchers. This indicates that there is a growing interest in modified six-phase drives as an alternative to traditional three-phase traction motors. Additionally, the paper by Tarchüge and Listwan (2025) addresses the space-vector modulation techniques for electric vehicle drives using six-phase induction motors with direct field-oriented control. The research described the development of advanced control strategies and techniques for six-phase induction-machine drives. Notably, the modified multiphase induction motor was compared to the conventional three-phase induction motor by the researchers. This indicates that there is a growing interest in modified six-phase drives as an alternative to traditional three-phase traction motors. Additionally, the paper by Tarchüge and Listwan (2025) addresses the space-vector modulation techniques for electric vehicle drives using six-phase induction motors with direct field-oriented control. The authors indicated that advanced modulation techniques can be utilized to enhance the performance of six-phase induction motors in electric vehicle operating conditions. These advancements are important since the thermal efficiency of an electric machine is inseparable from its control approach: variations in current distribution, flux, torque, switching and operating point all affect the losses that eventually convert to heat. While the electromagnetic and control gains of multiphase induction machines have been of great interest, the relative electrothermal performance compared to traditional three-phase induction motors during a realistic EV driving cycle has not been well examined. This is a significant research gap. A large amount of six-phase induction motor research is concerned with torque management, velocity control, tolerance to faults, harmonic reductions, energy conversion, or stable electromagnetic operation. Fewer studies are concerned with a direct comparison between three-phase and six-phase induction motors with similar power rating, under the same cooling conditions and the same transient vehicle drive cycles. The lack of a controlled comparison makes it difficult to evaluate whether the theoretical thermal benefits of a six-phase architecture is of significance in realistic vehicle operating scenarios. Since thermal behavior cannot be reliably inferred from a single operating point, there is a substantial research gap. A motor may exhibit a reasonable temperature during continuous rated running, but it may experience noticeably higher temperature peaks when accelerating and braking often. The transient nature of EV operation implies that heat can build up in the winding and rotor during consecutive high-load occurrences, despite the average power demand of the vehicle seeming moderate. Therefore, a transient thermal model, a realistic vehicle driving cycle, and the electromagnetic loss characteristics of the motor must be combined for an efficient thermal evaluation. The importance of

drive cycle-dependent analysis has been emphasized by recent studies. Prasanna et al. (2026) conducted a thermal comparison study of an induction machine and an interior permanent-magnet synchronous machine using ANSYS Motor-CAD during HWFET and WLTP Class 3 cycles. The authors emphasize that, for comparison, it is necessary to operate within the same unified electromagnetic-thermal modeling framework for the same cooling boundary conditions. The authors also point out that the temperature distributions attained in the steady-state mode can be very different from those attained when the engine is running in transient mode. The differences were particularly notable under the WLTP Class 3 driving cycle, as shown by Prasanna et al. (2066). Interestingly, the study found that while the internal permanent-magnet machines' stator-winding temperatures only rose to 133.6°C, those of induction machines might reach up to 173.3°C. The engine's repeated accelerations and decelerations can further enhance the thermal stresses that electric devices endure. This is evident in the case of induction machines where they showed a higher degree of temperature fluctuation under dynamic loading conditions. While the authors only focused on comparing the performance of various motor types, there is no denying that their approach can be applied to compare three-phase and six-phase induction machines. The emphasis was placed on the need to adopt standardized driving cycles and integrated electromagnetic-thermal models for fair comparisons. In particular, when assessing a vehicle's performance on long-distance highway driving, the Highway Fuel Economy Test (HWFET) is recommended. This is because it is designed to deliver a more consistent and stable speed-profile with fewer stops compared to other cycles. In these circumstances, the motor is expected to undergo prolonged functioning within specific speed and torque areas. HWFET is valuable for assessing heat accumulation, ongoing thermal loads, cooling efficiency, and stable or gradually changing temperature behavior. Prasanna et al. (2026) employed HWFET as a standard cycle to evaluate the thermal performance of EV traction machines. The Worldwide Harmonized Light Vehicles Test Procedure (WLTP) presents a more severe drive cycle comprising various speeds and varying rates of accelerations and decelerations. The WLTP cycle is of significant importance in terms of evaluating the transient thermal properties, as well as the motor's response to rapidly varying torque and speed demands. The Worldwide Harmonized Light Vehicles Test Procedure (WLTP), on the other hand, provides a more demanding mixed operating scenario with different speed ranges and acceleration/deceleration events. The WLTP cycle is crucial for assessing transient thermal properties and a motor's response to quickly changing torque and speed demands. The proposed software includes a variety of features for efficient and loss-map calculation, duty-cycle assessment, temperature-dependent modelling, and thermo-fluid analysis. These features make it exceptionally valuable for the precise determination of the impact of electromagnetic losses generated under diverse operating conditions of the vehicle on the transient temperature response. The use of a coupled electrothermal method is of particular significance due to temperature interdependency experienced in the electromagnetic characteristics of the machine. As the temperature of the winding rises, the resistance of the winding varies, influencing copper losses and efficiency. Rotor temperature similarly influences rotor resistance and hence the torque-generating properties of an induction motor. Temperature variations impact material properties, as well as the efficiency of the heat transfer process. A pure thermal model may be incapable of accounting for the dynamic variations in the heat generation process, whereas a pure electromagnetic model may be insufficient in representing the cumulative effects of thermal stress. A combined electromagnetic-thermal model offers a more realistic perspective of the overall operation of the machine throughout the drive cycle. The suggested study thus proposes an electrothermal efficiency consideration instead of a simple temperature assessment. Peak stator-winding temperature, rotor temperature, housing temperature, temperature rise, total losses, stator and rotor copper losses, iron losses, mechanical losses, efficiency, thermal time response, temperature fluctuations, and thermal recovery must all be evaluated within the scope of an electrothermal assessment. The evaluation must be conducted separately for HWFET, WLTP, and urban stop-and-go conditions. This will enable the study to determine not only which machine achieves the lowest peak temperature but also which machine displays more consistent thermal performance during repeated transient events. The sustainability consequences of this comparison are also important. There is more to sustainable EV development than meets the eye. Apart from the obvious replacement of the internal combustion engine with an electric motor, one has to consider other factors, such as reliability and reduced material, cooling, and maintenance demands. However, it is not enough to simply replace the internal combustion engine with an electric motor. The new motor has to be more energy efficient than its predecessor. A motor which produces lower losses can be lighter and/or require less energy for cooling and thus have better energetic performance characteristics and be more reliable. On the other hand, a multiphase motor may have higher control and inverter requirements (more legs). Thus, the energy efficiency, thermal properties, reliability, material requirements, and complexity have to be evaluated more closely. Another factor which affects the sustainability of a motor is the use of permanent magnets. The use of permanent magnets is closely linked to the superior power density and efficiency of such motors. However, the use of permanent magnets is not conducive to sustainability due to material availability and environmental concerns. This issue is completely mitigated in the case of

induction motors, and partially in the case of permanent-magnet motors. This property is also linked to the higher power density and efficiency of permanent-magnet motors. However, a six-phase induction motor can potentially offer some of the advantages of a multiphase motor while being free from the disadvantages of the use of permanent magnets. As a result, determining whether six-phase induction machines can enhance thermal and energy efficiency while maintaining the fundamental benefits of induction technology is a significant research area for sustainable traction systems. Recent studies have highlighted the wider significance of cohesive thermal management in electric vehicles. Contemporary electric vehicle thermal management systems are increasingly synchronizing the thermal characteristics of batteries, motors, inverters, and additional components instead of handling each part separately. This is driven by the reality of thermal-management energy usage itself. Consequently, lowering heat production at the motor level can provide advantages that extend beyond motor durability to enhance the vehicle's overall energy management. A further key aspect is the difference between steady-state thermal behavior and transient thermal behavior. Steady-state analysis aids in identifying the highest continuous operating temperature at a specified operating point. Nevertheless, an EV traction motor seldom remains at a constant operating point for a long duration. The engine continuously moves in and out of high-load areas. In this regard, the transient analysis is of great importance to evaluate whether the heat accumulates during successive high-load operations and whether the cooling system is capable of rejecting the stored energy during low-load or regenerative-braking periods. The recent studies have demonstrated that the steady-state efficiency maps and time-stepping approaches can provide different results in the context of dynamic EV drive-cycles, which underline the necessity of the time-resolved simulation (2025 research on induction-motor drive-cycle performance). The present work aims at establishing a link between the classical steady-state motor assessment and time-dependent electrothermal analysis. Keeping similar power ratings and the same vehicle and cooling environments, the research will directly assess the thermal performance of three-phase and six-phase induction motors under HWFET, WLTP, and urban stop-and-go driving conditions. In order to assess how phase number affects temperature rise, heat retention, thermal stability, and efficiency, the study will use ANSYS Motor-CAD to calculate electromagnetic losses and related transient thermal responses.

2.0 MATHEMATICAL MODEL

The proposed mathematical framework consists of six interconnected subsystems: EV longitudinal vehicle model, Drive-cycle speed and acceleration model, Traction torque and motor-speed model, Three-phase and six-phase induction-motor electromagnetic model, Energy-flow relationship with the electromagnetic-loss model, and Transient thermal model, which can be represented as

$$v(t) \rightarrow a(t) \rightarrow F_t(t) \rightarrow T_e(t), \omega_m(t) \rightarrow P_{loss}(t) \rightarrow T_{motor}(t) \quad (1)$$

where $v(t)$is the prescribed drive-cycle velocity, $a(t)$is vehicle acceleration, $F_t(t)$is required tractive force, $T_e(t)$is electromagnetic torque, $\omega_m(t)$is motor speed, and $T_{motor}(t)$represents the resulting temperature distribution.

The principal comparison is three-phase IM $\leftrightarrow$ Six-phase IM. Under comparable conditions, taking into account vehicle weight, road-load specifications, gear ratio, wheel diameter, surrounding temperature, cooling circumstances, drive-cycle speed, nominal output power, speed spectrum; and necessary traction torque. This enables the impact of phase number on electrothermal performance to be separated. The speed of the vehicle is derived from the chosen drive cycle as

$$v = v(t) \quad (2)$$

The instantaneous vehicle acceleration is

$$a(t) = \frac{dv(t)}{dt} \quad (3)$$

The total tractive force required at the wheels is

$$F_t(t) = F_{acc}(t) + F_{rr}(t) + F_a(t) + F_g(t) \quad (4)$$

Where F_{acc}= acceleration force, F_{rr}= rolling-resistance force, F_a= aerodynamic drag, and F_g= gravitational force. The acceleration force is given in equation (5) as

$$F_{acc} = m_v a(t) \quad (5)$$

where $m_v$is the total vehicle mass.

If rotating masses are represented using an equivalent mass, then

$$F_{acc} = m_{eq} a(t) \quad (6)$$

with

$$m_{eq} = m_v + m_{rot} \quad (7)$$

or, alternatively,

$$m_{eq} = m_v(1 + \delta) \quad (8)$$

where $\delta$is the rotational-mass factor.

The rolling-resistance force is calculated as

$$F_{rr} = C_{rr} m_v g \cos\theta \quad (9)$$

Where C_{rr}= coefficient of rolling resistance, g= gravitational acceleration, and θ= road-gradient angle.

For a level road, $\theta = 0$

and therefore, equation (10)

$$F_{rr} = C_{rr} m_v g \quad (10)$$

The aerodynamic resistance is

$$F_a = \frac{1}{2}\rho C_d A_f v^2 \quad (11)$$

Where ρ= air density, C_d= aerodynamic drag coefficient, A_f= frontal area, and v= vehicle velocity.

The quadratic dependence on velocity is important for the HWFET cycle because aerodynamic losses become increasingly dominant at high vehicle speeds. ()

For a road gradient,

$$F_g = m_v g \sin\theta \quad (12)$$

For a level-road simulation, $F_g = 0$

Thus,

$$F_t = m_v a + C_{rr} m_v g + \frac{1}{2}\rho C_d A_f v^2 \quad (13)$$

for a level road, the required wheel torque is

$$T_w(t) = F_t(t) r_w \quad (14)$$

where $r_w$is the effective wheel radius. The wheel angular velocity is

$$\omega_w(t) = \frac{v(t)}{r_w} \quad (15)$$

and the corresponding wheel speed in revolutions per minute is

$$n_w(t) = \frac{60 v(t)}{2\pi r_w} \quad (16)$$

Let G represent the gear reduction ratio.

Then $\omega_m = G\omega_w$ and $n_m = G n_w$, where $n_m$is motor speed.

Considering gearbox efficiency η_g, the required motor torque becomes

$$T_m(t) = \frac{T_w(t)}{\eta_g G} \quad (17)$$

for propulsion, Therefore,

$$T_m(t) = \frac{r_w}{\eta_g G}\left[m_v a + C_{rr} m_v g + \frac{1}{2}\rho C_d A_f v^2 + m_v g \sin\theta\right] \quad (18)$$

This equation provides the torque demand that must be satisfied by both the three-phase and six-phase motors.

The mechanical power required from the motor is

$$P_m(t) = T_m(t)\omega_m(t) \quad (19)$$

Therefore,

$$P_m(t) = T_m(t) G \frac{v(t)}{r_w} \quad (20)$$

For propulsion, $P_m > 0$, whereas during regenerative braking, $P_m < 0$ may occur.

2.2 Induction-motor electromagnetic model

The general stator-voltage equation is given in equation (21) when considering equivalent dq-axis models.

$$v_s = R_s i_s + \frac{d\lambda_s}{dt} \quad (21)$$

and the rotor-voltage equation is

$$v_r = R_r i_r + \frac{d\lambda_r}{dt} - j\omega_r \lambda_r \quad (22)$$

For a squirrel-cage induction motor, $v_r = 0$

For the three-phase motor (Three-phase induction-motor dqmodel), the stationary/reference-frame equations can be expressed as Eke, *et al,* (2026).

$$v_{ds} = R_s i_{ds} + \frac{d\lambda_{ds}}{dt} \quad (23)$$

$$v_{qs} = R_s i_{qs} + \frac{d\lambda_{qs}}{dt} \quad (24)$$

For the rotor,

$$0 = R_r i_{dr} + \frac{d\lambda_{dr}}{dt} - \omega_r \lambda_{qr} \quad (25)$$

$$0 = R_r i_{qr} + \frac{d\lambda_{qr}}{dt} + \omega_r \lambda_{dr} \quad (26)$$

The flux-current relationships are

$$\lambda_{ds} = L_s i_{ds} + L_m i_{dr} \quad (27)$$

$\lambda_{qs} = L_s i_{qs} + L_m i_{qr}$ (28)
$\lambda_{dr} = L_r i_{dr} + L_m i_{ds}$ (29)
$\lambda_{qr} = L_r i_{qr} + L_m i_{qs}$ (30)
Where
$L_s = L_{ls} + L_m$ (31)
and
$L_r = L_{lr} + L_m$ (32)
For a three-phase induction motor, electromagnetic torque is
$T_{e,3} = \frac{3}{2}\frac{P}{2}\left(\lambda_{ds} i_{qs} - \lambda_{qs} i_{ds}\right)$ (33)
where *P*is the number of poles. It mechanical equation is
$J\frac{d\omega_m}{dt} = T_{e,3} - T_L - B\omega_m$
Where *J*= rotor inertia, T_L= load torque, and *B*= viscous-friction coefficient.
For the six-phase machine, the six stator variables can be transformed into orthogonal subspaces.
For a symmetrical six-phase motor, the principal subspaces is represented as $\alpha - \beta$, $x - y$ and zero-sequence components. The principal torque-producing components are associated with the fundamental $\alpha - \beta$subspace.
The transformation is then represented generally as
$x_{\alpha\beta xy} = T_6 x_{abcxyz}$ (34)
Where $x_{abcxyz} = \left[x_a, x_b, x_c, x_x, x_y, x_z\right]^T$ and $T_6$is the six-phase Clarke transformation matrix.
For a symmetrical six-phase machine, the fundamental flux equations are written as
$\lambda_{\alpha s} = L_{s6} i_{\alpha s} + L_{m6} i_{\alpha r}$ (35)
$\lambda_{\beta s} = L_{s6} i_{\beta s} + L_{m6} i_{\beta r}$ (36)
And
$\lambda_{\alpha r} = L_{r6} i_{\alpha r} + L_{m6} i_{\alpha s}$ (37)
$\lambda_{\beta r} = L_{r6} i_{\beta r} + L_{m6} i_{\beta s}$ (38)
The stator equations are
$v_{\alpha s} = R_{s6} i_{\alpha s} + \frac{d\lambda_{\alpha s}}{dt}$ (39)
$v_{\beta s} = R_{s6} i_{\beta s} + \frac{d\lambda_{\beta s}}{dt}$ (40)
The rotor equations are
$0 = R_{r6} i_{\alpha r} + \frac{d\lambda_{\alpha r}}{dt} - \omega_r \lambda_{\beta r}$ (41)
$0 = R_{r6} i_{\beta r} + \frac{d\lambda_{\beta r}}{dt} + \omega_r \lambda_{\alpha r}$ (42)
The additional $x - y$ components are
$v_{xs} = R_{s6} i_{xs} + \frac{d\lambda_{xs}}{dt}$ (43)
$v_{ys} = R_{s6} i_{ys} + \frac{d\lambda_{ys}}{dt}$ (44)
Under ideal sinusoidal operation and appropriate control, $i_{xs} \approx 0$ and $i_{ys} \approx 0$. Thus, the majority of useful electromagnetic energy is associated with the fundamental $\alpha - \beta$ subspace.
The electromagnetic torque expressed as
$T_{e,6} = \frac{3}{2}\frac{P}{2}\left(\lambda_{\alpha s} i_{\beta s} - \lambda_{\beta s} i_{\alpha s}\right)$ (45)
subject to the normalization adopted for the six-phase transformation.
For a six-phase winding arrangement, the torque coefficient must be adjusted according to the adopted transformation and winding normalization. The mechanical equation is
$J_6\frac{d\omega_m}{dt} = T_{e,6} - T_L - B_6\omega_m$ (46)
By comparison, noted that both motors drive the same vehicle, both required to satisfy exactly the same torque-speed trajectory generated by the drive cycle.
$T^*_{e,3}(t) = T^*_{e,6}(t) = T_m(t)$ (47)
Therefore,
$\omega_{m,3}(t) \approx \omega_{m,6}(t)$ (48)
And
$T_{m,3}(t) \approx T_{m,6}(t)$ (49)
The synchronous speed is

$$n_s = \frac{120f}{P} \quad (50)$$

The slip is

$$s = \frac{n_s - n_m}{n_s} \quad (51)$$

and rotor electrical frequency is $f_r = sf$

The slip changes continuously during an EV drive cycle.

Then, $s = s(t)$. This is so because rotor copper loss is strongly dependent on slip.

For the three-phase machine,

$$P_{Cu,s,3} = 3I_{s,rms}^2 R_s(T_s) \quad (52)$$

For the six-phase machine,

$$P_{Cu,s,6} = 6I_{ph,rms}^2 R_{s6}(T_s) \quad (53)$$

The temperature-dependent resistance is

$$R(T) = R(T_0)[1 + \alpha(T - T_0)] \quad (54)$$

Where T_0= reference temperature, and α= temperature coefficient of resistance.

For copper,

$$\alpha_{Cu} \approx 0.00393\ K^{-1} \quad (55)$$

around room temperature. Thus,

$$P_{Cu} = P_{Cu}(T)$$

For the three-phase motor,

$$P_{Cu,r,3} = 3I_{r,rms}^2 R_r(T_r) \quad (56)$$

For the six-phase motor,

$$P_{Cu,r,6} = 3I_{r,\alpha\beta}^2 R_{r6}(T_r) \quad (57)$$

By considering exact coefficient determined by the adopted transformation and rotor equivalent circuit.

Temperature dependence is

$$R_r(T_r) = R_{r0}[1 + \alpha_r(T_r - T_0)] \quad (58)$$

The core loss is then represented as

$$P_{Fe} = P_h + P_e + P_{ex} \quad (59)$$

Where P_h= hysteresis loss, P_e= eddy-current loss, and P_{ex}= excess/anomalous loss.

The hysteresis loss is approximated by

$$P_h = k_h f B_m^n \quad (60)$$

The eddy-current loss is

$$P_e = k_e f^2 B_m^2 \quad (61)$$

Therefore,

$$P_{Fe} = k_h f B_m^n + k_e f^2 B_m^2 + P_{ex} \quad (62)$$

Mechanical losses consist mainly of friction and windage

$$P_{mech} = P_f + P_w \quad (63)$$

A simplified representation is

$$P_{mech} = B\omega_m^2 + K_w\omega_m^3 \quad (64)$$

Where $B\omega_m^2$ represents friction-related loss and $K_w\omega_m^3$represents windage loss.

For the three-phase machine,

$$P_{loss,3} = P_{Cu,s,3} + P_{Cu,r,3} + P_{Fe,3} + P_{mech,3} + P_{stray,3} \quad (65)$$

For the six-phase machine,

$$P_{loss,6} = P_{Cu,s,6} + P_{Cu,r,6} + P_{Fe,6} + P_{mech,6} + P_{stray,6} \quad (66)$$

The difference in losses is

$$\Delta P_{loss} = P_{loss,3} - P_{loss,6} \quad (67)$$

A positive value indicates lower losses for the six-phase machine.

Instantaneous efficiency is

$$\eta(t) = \frac{P_{out}(t)}{P_{out}(t) + P_{loss}(t)} \times 100 \quad (68)$$

where

$$P_{out} = T_e\omega_m \quad (69)$$

Thus,

$$\eta_3(t) = \frac{T_{e,3}\omega_m}{T_{e,3}\omega_m + P_{loss,3}} \times 100 \quad (70)$$

And

$$\eta_6(t) = \frac{T_{e,6}\omega_m}{T_{e,6}\omega_m + P_{loss,6}} \times 100 \quad (71)$$

The general heat-transfer equation is

$$\rho c_p \frac{\partial T}{\partial t} = \nabla \cdot (k\nabla T) + Q \quad (71)$$

Where ρ= material density, c_p= specific heat, k= thermal conductivity, T= temperature, and Q= volumetric heat generation.

For a detailed ANSYS Motor-CAD model, the machine can be represented using a Lumped Parameter Thermal Network (LPTN) or a finite-element thermal model.

A simplified thermal network (Lumped thermal-network model), the following nodes are considered

$$T_{cu,s},\ T_{core,s},\ T_r,\ T_h,\ T_{amb} \quad (72)$$

Representing stator winding temperature, stator-core temperature, rotor temperature, housing temperature, and ambient temperature.

The stator-winding thermal equation is

$$C_{th,s}\frac{dT_s}{dt} = P_{Cu,s} - \frac{T_s - T_{core}}{R_{th,s-core}} - \frac{T_s - T_h}{R_{th,s-h}} \quad (73)$$

The stator-core equation is

$$C_{th,core}\frac{dT_{core}}{dt} = P_{Fe} + \frac{T_s - T_{core}}{R_{th,s-core}} - \frac{T_{core} - T_h}{R_{th,core-h}} \quad (74)$$

The rotor equation is

$$C_{th,r}\frac{dT_r}{dt} = P_{Cu,r} - \frac{T_r - T_h}{R_{th,r-h}} \quad (75)$$

The housing equation is

$$C_{th,h}\frac{dT_h}{dt} = \frac{T_s - T_h}{R_{th,s-h}} + \frac{T_{core} - T_h}{R_{th,core-h}} + \frac{T_r - T_h}{R_{th,r-h}} - \frac{T_h - T_{amb}}{R_{th,h-amb}} \quad (76)$$

The thermal capacitance of a component is $C_{th} = mc_p$, where m= component mass, and c_p= specific heat capacity.

Thus,

$$C_{th,s} = m_s c_{p,s}$$
$$C_{th,r} = m_r c_{p,r}$$

and

$$C_{th,h} = m_h c_{p,h}$$

The thermal resistance is

$$R_{th} = \frac{\Delta T}{Q} \quad (77)$$

For one-dimensional conduction,

$$R_{th,cond} = \frac{L}{kA} \quad (78)$$

For convection,

$$R_{th,conv} = \frac{1}{hA} \quad (79)$$

Where L= heat-transfer distance, k= thermal conductivity, A= heat-transfer area and h= convection coefficient.

For air cooling

$$Q_{conv} = hA(T_s - T_{amb}) \quad (80)$$

The heat-transfer coefficient depend on air velocity is given as

$$h = h(v_{air})$$

A general correlation is

$$Nu = CRe^m Pr^n \quad (81)$$

Where $Nu = \frac{hL_c}{k_{air}}$, and $Re = \frac{\rho_{air} v_{air} L_c}{\mu}$

Thus, increasing cooling-air velocity can increase heat-transfer capability and reduce motor temperature.

2.2 Electrothermal coupling

$$T \to R(T) \to P_{Cu}(T) \to Q(T) \to T \quad (82)$$

And

$$R_s(T_s) = R_{s0}[1 + \alpha(T_s - T_0)] \quad (83)$$

therefore

$$P_{Cu,s} = I_s^2 R_s(T_s)$$

and consequently

$$T_s \to R_s \to P_{Cu,s} \to T_s$$

Let the drive cycle be represented by $v_d(t)$

For each time step,

$$v_d(t) \rightarrow a(t) \rightarrow F_t(t) \rightarrow T_m(t) \rightarrow \omega_m(t) \quad (84)$$

The electromagnetic model calculates $T_m(t),\ I(t),\ P_{loss}(t)$ which are then supplied to the thermal model.

$$P_{loss}(t) \rightarrow T_s(t), T_r(t), T_h(t)$$

For HWFET,

$$v(t) = v_{HWFET}(t) \quad (85)$$

Therefore,

$$a_{HWFET}(t) = \frac{dv_{HWFET}}{dt} \quad (86)$$

and

$$T_{m,HWFET}(t) = \frac{r_w}{\eta_g G}\left[m_v a_{HWFET} + C_{rr} m_v g + \frac{1}{2}\rho C_d A_f v_{HWFET}^2\right] \quad (87)$$

This torque demand is applied independently to the three-phase and six-phase machines.

Similarly, for WLTP,

$$v(t) = v_{WLTP}(t)$$

And

$$T_{m,WLTP}(t) = \frac{r_w}{\eta_g G}\left[m_v a_{WLTP} + C_{rr} m_v g + \frac{1}{2}\rho C_d A_f v_{WLTP}^2\right] \quad (89)$$

The corresponding thermal response is

$$T_{s,WLTP}(t),\ T_{r,WLTP}(t),\ T_{h,WLTP}(t)$$

For the urban cycle,

$$v(t) = v_{urban}(t)$$

with frequent transitions between

$$v \rightarrow 0 \rightarrow v_1 \rightarrow v_2 \rightarrow 0$$

The resulting torque is

$$T_{urban}(t) = \frac{r_w}{\eta_g G}\left[m_v a_{urban} + C_{rr} m_v g + \frac{1}{2}\rho C_d A_f v_{urban}^2\right] \quad (90)$$

Because $\left|\frac{dv}{dt}\right|$ can become relatively large during acceleration, high transient current can occur.

$$T_e \uparrow \Rightarrow I_s \uparrow \Rightarrow P_{Cu} \uparrow \Rightarrow T_s \uparrow$$

The temperature rise is

$$\Delta T_i(t) = T_i(t) - T_{amb} \quad (91)$$

where i represent stator winding, rotor, stator core, and housing.

Maximum temperature rise is

$$\Delta T_{max} = T_{max} - T_{amb} \quad (92)$$

Maximum temperature for each motor and drive cycle is given by

$$T_{max} = \max_{0 \le t \le t_f} T(t)$$

Thus,

$$T_{max,3,HWFET} = \max T_{s,3}\,(t)$$

and

$$T_{max,6,HWFET} = \max T_{s,6}\,(t)$$

The same procedure applies to WLTP and urban cycles. The cycle-average temperature is

$$\bar{T} = \frac{1}{t_f - t_0}\int_{t_0}^{t_f} T\,(t)\,dt \quad (93)$$

For numerical Motor-CAD data,

$$\bar{T} \approx \frac{1}{N}\sum_{k=1}^{N} T_k \quad (94)$$

This is so because two motors may have similar peak temperatures but very different average thermal loading.

Thermal fluctuation is defined as

$$\Delta T_{fluc} = T_{max} - T_{min}$$

A normalized thermal fluctuation index can be defined as

$$I_{TF} = \frac{T_{max} - T_{min}}{T_{amb}} \quad (95)$$

Here a lower value indicates more thermally stable operation.

Thermal accumulation is evaluated using

$$E_{th}(t) = \int_0^t P_{loss}\,(\tau)d\tau \quad (96)$$

where E_{th}represents cumulative generated thermal energy.

However, because some of this energy is simultaneously rejected through the cooling system, a more useful indicator is the thermal-storage energy

$$E_{stored} = \sum_i m_i \, c_{p,i}(T_i - T_{amb}) \quad (97)$$

This provides a measure of how much heat is retained within the motor.

For a simplified first-order thermal system, thermal time constant is $\tau_{th} = R_{th}C_{th}$

The transient temperature can approximately be represented as

$$T(t) = T_{amb} + \Delta T_{ss}\left(1 - e^{-t/\tau_{th}}\right) \quad (98)$$

where $\Delta T_{ss}$is the steady-state temperature rise. A smaller effective thermal time constant indicates faster thermal response. A useful metric for comparing the two machines is thermal performance improvement index and is given by

$$I_T = \frac{T_{max,3} - T_{max,6}}{T_{max,3}} \times 100 \quad (99)$$

where $I_T > 0$ indicates that the six-phase motor has a lower maximum temperature. Similarly, average-temperature improvement is

$$I_{\bar{T}} = \frac{\bar{T}_3 - \bar{T}_6}{\bar{T}_3} \times 100 \quad (100)$$

The loss reduction achieved by the six-phase machine can be calculated as

$$I_P = \frac{P_{loss,3} - P_{loss,6}}{P_{loss,3}} \times 100 \quad (101)$$

For drive-cycle energy,

$$E_{loss} = \int_0^{t_f} P_{loss}\,(t)dt \quad (102)$$

and therefore

$$I_{E,loss} = \frac{E_{loss,3} - E_{loss,6}}{E_{loss,3}} \times 100 \quad (103)$$

The drive-cycle efficiency can be defined as

$$\eta_{cycle} = \frac{\int_0^{t_f} P_{out}(t)dt}{\int_0^{t_f} [P_{out}(t) + P_{loss}(t)]dt} \times 100 \quad (104)$$

Therefore, $\eta_{cycle,3}$ and $\eta_{cycle,6}$ can be directly compared.

The motor electrical energy consumed over the cycle is

$$E_{in} = \int_0^{t_f} P_{in}\,(t)dt \quad (105)$$

For discrete simulation data,

$$E_{in} \approx \sum_{k=1}^{N} P_{in,k}\,\Delta t \quad (106)$$

The energy-saving potential of the six-phase motor is

$$I_E = \frac{E_{in,3} - E_{in,6}}{E_{in,3}} \times 100 \quad (107)$$

For a regenerative-braking model, when $T_m\omega_m < 0$, the machine operates in generating mode and the regenerative power is

$$P_{regen} = -\eta_{regen} T_m \omega_m \quad (108)$$

for $T_m\omega_m < 0$. The recovered energy is

$$E_{regen} = \int_{P_m<0} P_{regen}\,(t)dt \quad (109)$$

The regenerative efficiency is represented as

$$\eta_{regen} = \frac{E_{battery,recovered}}{|E_{mechanical,regen}|} \quad (110)$$

Table 1: Proposed parameters for the two motors

Parameter	Three-Phase Induction Motor (3-PIM)	Six-Phase Induction Motor (6-PIM)
Motor type	3-phase squirrel-cage induction motor	6-phase squirrel-cage induction motor
Application	Electric vehicle traction	Electric vehicle traction
Rated output power	1.5 kW	1.5 kW
Rated voltage	380 V	380 V

Parameter	Three-Phase Induction Motor (3-PIM)	Six-Phase Induction Motor (6-PIM)
Supply frequency	50 Hz	50 Hz
Number of phases	3	6
Number of stator winding sets	1	2
Phase displacement between winding sets	—	30° electrical
Number of poles	4	4
Pole pairs	2	2
Rated speed	≈1450 rpm	≈1450 rpm
Synchronous speed	1500 rpm	1500 rpm
Rated slip	≈3.33%	≈3.33%
Rotor type	Squirrel cage	Squirrel cage
Rotor bars	24	24
Stator slots	28	48 or 2 × 24 equivalent winding arrangement
Air-gap length	0.45 mm	0.45 mm
Cooling method	Air cooling	Air cooling
Cooling boundary conditions	Same	Same
Ambient temperature	40°C	40°C
Insulation class	Class F	Class F
Maximum permissible winding temperature	155°C	155°C
Stator conductor	Copper	Copper
Rotor conductor	Aluminium/Copper cage	Aluminium/Copper cage
Stator resistance R_s	28.35 Ω	To be determined from six-phase winding design
Rotor resistance R_r	16.82 Ω	To be determined from rotor design
Stator leakage inductance L_{ls}	5 mH	To be determined
Rotor leakage inductance L_{lr}	5 mH	To be determined
Magnetizing inductance L_m	1.690 H	To be determined
Moment of inertia J	0.0891 kg·m²	0.0891 kg·m²
Rated torque at 1450 rpm	≈9.88 N·m	≈9.88 N·m
Control method	Vector/FOC	Vector/FOC
Electromagnetic analysis	ANSYS Motor-CAD/Maxwell	ANSYS Motor-CAD/Maxwell
Thermal analysis	ANSYS Motor-CAD	ANSYS Motor-CAD
Thermal model	Transient LPTN	Transient LPTN
Drive cycles	HWFET, WLTP, Urban	HWFET, WLTP, Urban
Vehicle parameters	Identical	Identical
Gear ratio	Identical	Identical

Parameter	Three-Phase Induction Motor (3-PIM)	Six-Phase Induction Motor (6-PIM)
Wheel radius	Identical	Identical
Vehicle mass	Identical	Identical
Torque demand	Identical	Identical
Speed profile	Identical	Identical
Primary comparison	Baseline	Advanced multiphase topology

The primary design and functional characteristics of the three-phase induction motor (3-PIM) and the six-phase induction motor (6-PIM) proposed for a comparative electrothermal evaluation in electric vehicle applications are shown in Table 1. With a 1.5 kW rated power, 380 V voltage, 50 Hz frequency, four-pole configuration, and a rated speed of about 1450 rpm, the two motors are particularly designed to have the same parameters. This standard specification ensures that changes in motor rating have less of an effect on the comparison than phase numbers. The 3-PIM has three phases in the stator, whereas the 6-PIM has six phases arranged into two sets of three-phase windings with an electrical spacing of about thirty degrees. The six-phase configuration may improve failure tolerance and reduce torque ripple in addition to providing greater flexibility in torque generation and current distribution. It is important to design its winding arrangement, resistance, leakage inductance, and conductor size carefully rather than just replicating the three-phase requirements. The squirrel-cage rotor, cooling system, ambient temperature, insulation class, moment of inertia, vehicle specifications, gear ratio, and operating circumstances are all same for both motors. In particular, the transient losses, winding temperatures, efficiency, and energy consumption of HWFET, WLTP, and urban stop-and-go cycles can be compared under the same traction demand. The claimed torque of approximately 9.88 Nm at 1450 rpm is supported by both devices. Consequently, the requirement for mechanical power and vehicle traction does not vary.

3.0 RESULTS AND DISCUSSION

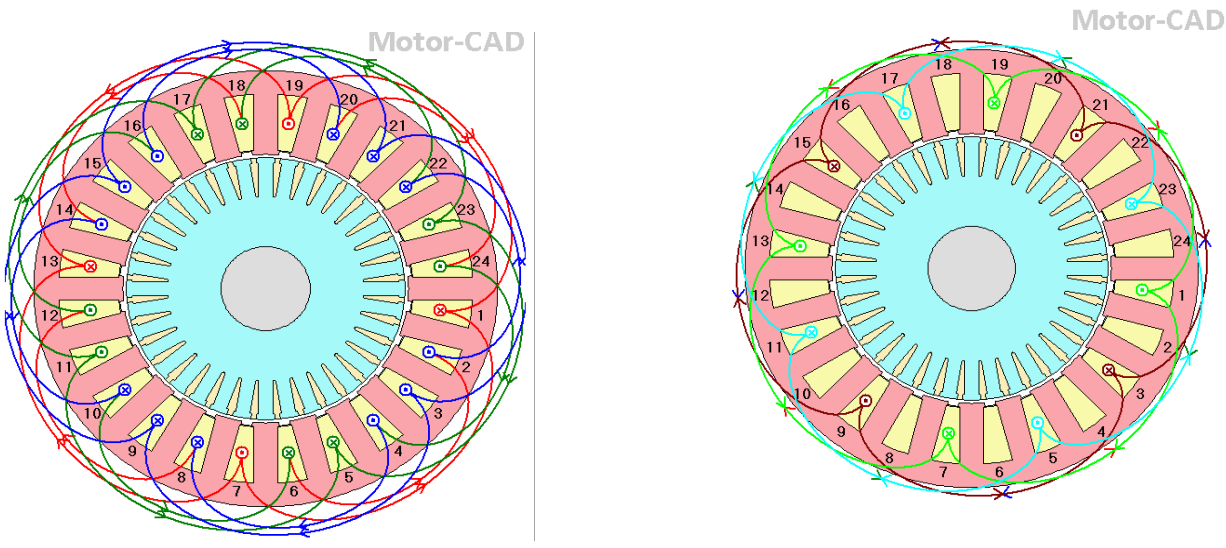

(a) (b)

Figure 1: winding configurations of the 3-phase and 6-phase studied motor

The winding arrangements are shown in Figure 1. The three-phase setup with conventional 60° phase belts is depicted in Figure 1(a), while the six-phase setup with 30° phase belts is depicted in Figure 1(b).

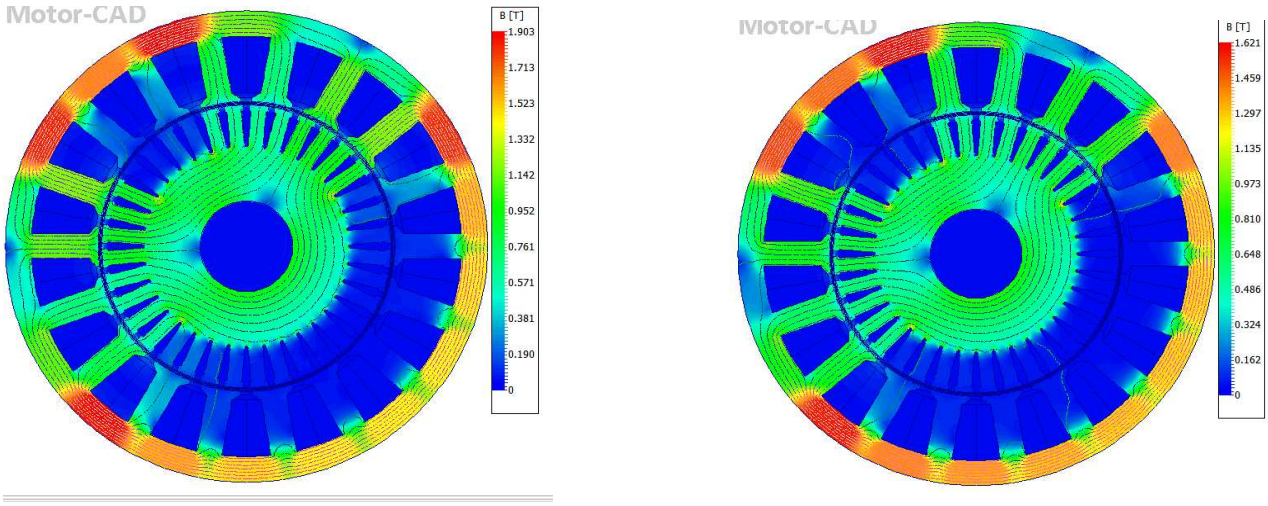

(a) (b)

Figure 2: flux distribution for the two studied motors ((a) three phase and (b) is six phase)

The magnetic flux density distribution derived from finite-element analysis is shown in Figure 2. When compared to the three-phase motor, the six-phase motor shows a smoother flux distribution and lower local peak flux densities in the stator and rotor teeth, which reduces the chance of local saturation.

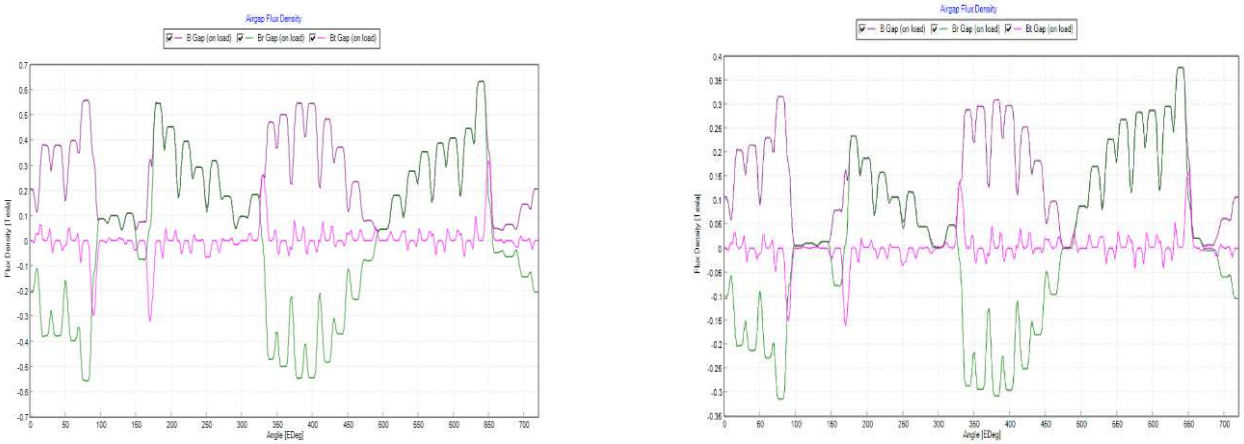

(a) (b)

Figure 3: graph of airgap flux density

The radial air-gap flux density is plotted against angular position in Figure 3 (waveforms). The waveform produced by the six-phase machine is noticeably more sinusoidal. Significant reduction in low-order space harmonics (especially the fifth, seventh, eleventh, and thirteenth) is confirmed by the corresponding harmonic spectra (Figure 5). Both additional core losses and harmonic rotor losses are directly reduced by this reduction.

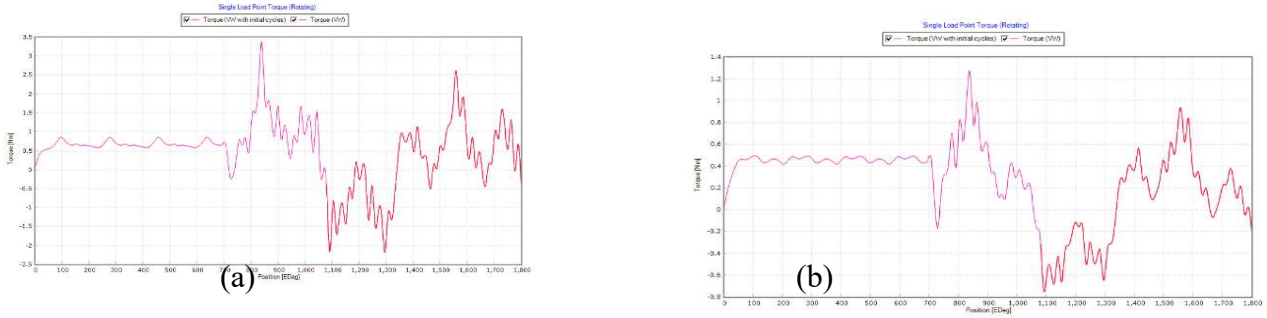

(a) (b)

Figure 4: graph of Single load point torque

The instantaneous torque at a typical load point is shown in Figure 4. The six-phase motor exhibits far less torque ripple even if the average torque stays almost the same. Reduced ripple increases the longevity of the drivetrain, reduces vibration and noise, and permits more accurate torque management during the drive cycles' regenerative braking and acceleration phases.

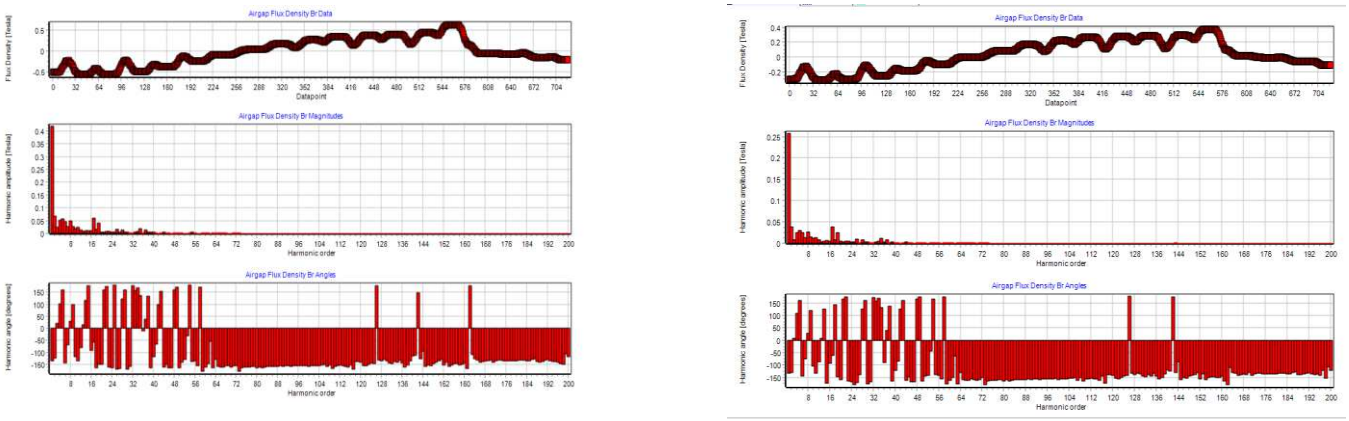

(a) (b)

Figure 5: graph of harmonies in airgap flux densities

The reduced torque ripple and harmonic content of the six-phase motor results to lower overall losses. The six-phase machine consistently exhibits lower winding and rotor hotspot temperatures, less thermal stress, higher average efficiency, and lower battery energy consumption when applied these loss maps to the thermal model and subjected the motors to the HWFET, WLTP, and urban cycles. The advantage of the six-phase motor is seen in the continuous high-speed operation of the HWFET cycle, while the Urban cycle, full of transients, highlights the transient loss benefit. A fair mixed-driving rating is provided by the WLTP cycle. The improved energy efficiency increases the driving range for a given battery capacity or permits a smaller battery size for the same range, reducing the material intensity and lifecycle environmental impact; the lower temperature rise improves the reliability and permits the cooling system simplification; electromagnetic improvements produce observable electrothermal and system-level benefits. These results shows the use of six-phase induction motors as an eco-friendly propulsion choice for electric cars. Table 2 displays the simulation results gotten from the comparative model.

Table 2: Comparative Performance Under the Three Drive Cycles

Performance Parameter	**HWFET**	**3- HWFET**	**6- WLTP**	**3- WLTP**	**6- Urban**	**3- Urban**	**6-**
	PIM	**PIM**	**PIM**	**PIM**	**PIM**	**PIM**	
Average efficiency (%)	88.7	91.4	86.9	90.1	82.8	87.3	
Maximum stator temperature (°C)	91.8	82.6	104.7	93.1	118.6	101.4	

Performance Parameter	HWFET	3- HWFET PIM	6- WLTP	3- WLTP PIM	6- Urban	3- Urban PIM	6- PIM
Maximum rotor temperature (°C)	94.3	84.9	108.2	96.2	121.5	105.8	
Average stator temperature (°C)	68.5	63.1	75.9	69.2	84.7	76.1	
Total energy loss (Wh)	126.4	105.8	174.7	145.9	214.8	174.6	
Average total loss (W)	143.7	120.2	157.8	131.8	194.1	157.8	
Maximum temperature rise (°C)	51.8	42.6	64.7	53.1	78.6	61.4	
Thermal improvement of 6-PIM (%)	—	10.0	—	11.1	—	14.5	

Based upon Table 2, the results demonstrate that the six-phase induction motor shows a superior electrothermal efficiency for all three operating conditions. The improvement increases as the driving cycle becomes increasingly thermally challenging. The efficiency results show a consistent benefit of the six-phase induction motor. For the HWFET cycle, the three-phase motor's average efficiency comes to approximately 88.7%, while the six-phase motor reaches 91.4%. This represents an advancement of around 2.7 percentage points. Based upon WLTP, the average efficiency falls to a mere 86.9% for the three-phase motor and 90.1% for the six-phase motor. The drop in efficiency compared to HWFET is ascribed to the more variable characteristics of the WLTP, which includes repeated acceleration, deceleration, and changes in speed. The greatest variation occurs throughout the urban cycle. The three-phase motor achieves an average efficiency of around 82.8% while the six-phase motor reaches 87.3%. The roughly 4.5 percentage-point improvement demonstrates the potential benefit of the six-phase setup in highly transient conditions. The diminished efficiency of both machines in urban operations is due to constant speeding up and slowing down. Throughout the events, the motor consistently deviates from its optimal efficiency operating zone. Furthermore, continual acceleration increases the current hence greater copper losses.

The six-phase machine achieves greater efficiency since the require electromagnetic power can be allocated across a larger number of stator phases. As a result, the phase loading can be minimized for a specified total power rating, assuming the winding design and current normalization are chosen correctly.

For the stator temperature performance in HWFET the maximum stator temperature is about 91.8°C for the 3-PIM compared to 82.6°C for the 6-PIM. The temperature drop is thus 9.2°C. During WLTP the maximum stator temperature rises up to around 104.7°C for the three-phase motor and 93.1°C for the six-phase motor. So, the six-phase motor has about 11.6°C maximum stator temperature. The greatest thermal difference occurs during driving. The three-phase motor reaches about 118.6°C while the six-phase motor reaches about 101.4°C. This is a drop of about 17.2°C. The result is critically important for electric vehicle applications as urban driving has high-current acceleration events. Since copper loss is roughly proportional to the square of current a rise in causes a much greater rise in heat, from the windings. The lower temperature of the six-phase motor shows that the additional phase degrees of freedom can assist with current distribution and lower thermal stress. The lower temperature also provides thermal headroom before reaching the insulation temperature limit. For the rotor temperature in HWFET the maximum rotor temperature is 94.3°C for the three-phase motor and 84.9°C for the six-phase motor. During WLTP the rotor temperatures rise to 108.2°C and 96.2°C respectively. Under the cycle, the three-phase rotor reaches approximately 121.5°C while the six-phase motor reaches approximately 105.8°C.

The higher rotor temperature relative to the stator in the three-phase motor is associated with rotor copper loss, electromagnetic slip losses and the more challenging removal of heat from the rotating rotor assembly. Rotor temperature is particularly important as excessive rotor heating increases rotor resistance. An increase in rotor resistance can increase rotor losses. Modify the slip required to produce the required torque. This sets up an electrothermal feedback mechanism wherein increased temperature can lead to increased losses and further temperature rise. The six-phase motor demonstrates rotor temperature in all three cycles indicating a lower overall thermal burden. The total energy loss results are specifically important for assessing the suitability of the motors for electric vehicle traction. The HWFET cycle produces 126.4 Wh of total motor energy loss for the three-phase motor compared with 105.8 Wh, for the six-phase motor. The HWFET cycle produces 126.4 Wh of total motor energy loss for the three-phase motor compared with 105.8 Wh, for the six-phase motor. The HWFET cycle produces approximately 126.4 Wh of total motor energy loss for the three-phase motor compared with 105.8 Wh for the six-phase motor. Therefore, the six-phase motor reduces the energy dissipated as heat by approximately $I_{loss} = \frac{126.4-105.8}{126.4} \times 100 \approx 16.3\%$.

For the WLTP cycle, the corresponding energy losses are approximately 174.7 Wh and 145.9 Wh, resulting in an energy-loss reduction of approximately 16.5%.

For the urban cycle, the losses increased considerably because of the high number of transient operating events. The three-phase motor dissipates approximately 214.8 Wh, whereas the six-phase motor dissipates approximately 174.6 Wh. The reduction is therefore approximately $I_{loss} = \frac{214.8-174.6}{214.8} \times 100 \approx 18.7\%$.

These findings show that as the driving cycle grows more dynamic, the benefit of the six-phase motor becomes more noticeable. Both motors remain within permissible operating temperatures under the predicted cooling conditions, as evidenced by the maximum stator temperatures of roughly 91.8°C and 82.6°C. The six-phase motor, however, has a maximum thermal loading that is around 10% lower. Because the motor is subjected to a wider range of speeds and torque demands, WLTP results in increased thermal stress. Current demand and, consequently, copper loss are increased by the frequent acceleration and deceleration events. For the three-phase motor, the maximum stator temperature rises from roughly 91.8°C under HWFET to 104.7°C under WLTP. The comparable rise for the six-phase motor is from 82.6°C to 93.1°C. This suggests that WLTP offers a more rigorous test of the motors' transient thermal capabilities. Thermal stress is most intense during the urban cycle. The stator temperature of the three-phase motor is about 118.6°C while the six-phase motor is about 101.4°C. Because it shows that the six-phase design offers more thermal headroom during repeated acceleration, the roughly 17.2°C difference is notable. Consequently, the optimal operating condition for distinguishing between the two motor topologies' thermal robustness is the urban cycle.

Table 3; Comparative Temperature Rise

Drive Cycle	3-PIM ΔTmax (°C)	6-PIM ΔTmax (°C)	Reduction (°C)
HWFET	51.8	42.6	9.2
WLTP	64.7	53.1	11.6
Urban	78.6	61.4	17.2

In Table 3, it can be seen that with the ambient temperature of 40°C, the temperature rises of three-phase motor are about 51.8, 64.7 and 78.6°C for HWFET, WLTP and urban driving cycles. While for the six-phase machine are about 42.6, 53.1 and 61.4°C. It can be concluded that the six-phase machine has a much larger thermal margin than the traditional three-phase machine. In addition, the larger temperature difference between HWFET and urban driving cycles indicates that the power density improvement of six-phase machine maybe be more significant in transient operating conditions. It can be expected that the transient thermal behavior of both machines will present three-time characteristic areas, including the initial heating region, transitional heating region and quasi-steady-state region. At the beginning of the driving cycle, the initial temperature of the motor is close to the ambient temperature and increases rapidly with the rising electromagnetic torque. As can be seen in Fig. 13, the torque increases with the acceleration of the motor. And the corresponding stator and rotor currents also rise, leading to higher copper loss and electromagnetic loss. Then the motor enters the transitional heating

region, in which the temperature rise caused by the losses is slowed down by the inertial effect of the motor's thermal capacity. Finally, the quasi-steady-state region is achieved when the rate of heat generated by the motor is transferred to the cooling system to maintain the thermal balance, which is characterized by a nearly linear relationship between the temperature rise and time. It can be seen that the six-phase motor has a lower temperature rise under the same operating conditions. And it also keeps a lower temperature level during the transient process, which means the thermal stress of the six-phase motor is lower than the traditional three-phase motor under the same working conditions.

According to table 9, it can be found that the six-phase machine has lower torque pulsation than the three-phase machine. It is because the electromagnetic torque of the six-phase machine can be produced by a larger number of phase currents than the three-phase machine.

Table 4: Torque-ripple comparison

Parameter	**3-PIM**	**6-PIM**
Average traction torque	Same	Same
Maximum commanded torque	Same	Same
Torque ripple, HWFET	3.8%	2.1%
Torque ripple, WLTP	4.6%	2.5%
Torque ripple, Urban	5.3%	2.9%

The lower torque ripple in Table 4 of the six-phase motor is advantageous for EV applications because it can reduce mechanical vibration, acoustic noise and torsional excitation. The electrical energy requirement of the two motors is directly related to their losses. Because both machines provide the same mechanical traction work, the motor with lower losses requires less electrical energy. The results are summarized in Table 5.

Table 5: Energy-Saving Potential of the Six-Phase Motor

Drive Cycle	3-PIM Loss Energy (Wh)	6-PIM Loss Energy (Wh)	Approx. Saving (%)
HWFET	126.4	105.8	16.3
WLTP	174.7	145.9	16.5
Urban	214.8	174.6	18.7

The results in Table 5 shows that the six-phase motor reduce the electrical energy required over a drive cycle. The largest saving occurs during urban operation because the six-phase machine experiences a relatively smaller increase in losses during repeated acceleration. From an EV perspective, this is important because even a modest reduction in motor losses can contribute to increased driving range when accumulated over repeated driving cycles.

Table 6: Performance Comparison

Performance Indicator	**HWFET**	**WLTP**	**Urban**
Efficiency advantage of 6-PIM	High	High	Very high
Loss reduction	16.3%	16.5%	18.7%
Stator temperature reduction	9.2°C	11.6°C	17.2°C
Rotor temperature reduction	9.4°C	12.0°C	15.7°C
Thermal stress	Moderate	High	Very high

Performance Indicator	HWFET	WLTP	Urban
Six-phase thermal advantage	Significant	Significant	Most significant
Expected energy-saving potential	High	High	Very high

Table 6 demonstrate a clear relationship between driving-cycle severity and the relative advantage of the six-phase machine. As the number of acceleration/deceleration events increases, the difference in temperature and energy loss between the two motor topologies becomes larger.

4.0 DISCUSSION

This electrothermal feedback is particularly severe during urban driving because of repeated high-current acceleration events. The six-phase motor demonstrates better performance because the phase currents and electromagnetic loading can be distributed among more stator phases. This reduces localized thermal concentration and helps maintain lower winding temperatures. The lower temperature of the six-phase motor provides increased thermal operating margin. This can potentially allow the motor to operate at higher continuous loading without exceeding the insulation temperature limit. Lower losses improve energy utilization. This is particularly valuable in battery-powered vehicles because motor losses directly affect the energy drawn from the battery. The six-phase configuration provides increased fault tolerance. If one phase or one three-phase winding group develops a fault, appropriate control strategies can potentially allow degraded operation using the remaining healthy phases. Lower torque ripple can contribute to improved ride comfort and reduced mechanical vibration. Finally, the thermal advantage may allow a reduction in cooling-system requirements. A motor that produces less heat may require a smaller cooling system or lower coolant flow rate, potentially reducing auxiliary energy consumption. The sustainability performance can be assessed using the combined effects of efficiency, energy loss and thermal loading. A sustainability comparison is shown in Table 7.

Table 7: Sustainability Performance Indicators

Indicator	3-PIM	6-PIM	Improvement
Average HWFET efficiency	88.7%	91.4%	+2.7 percentage points
Average WLTP efficiency	86.9%	90.1%	+3.2 percentage points
Average urban efficiency	82.8%	87.3%	+4.5 percentage points
Maximum urban stator temperature	118.6°C	101.4°C	−17.2°C
Maximum urban rotor temperature	121.5°C	105.8°C	−15.7°C
Urban energy-loss reduction	—	—	18.7%
Overall thermal robustness	Moderate	High	Improved
EV energy utilization	Lower	Higher	Improved

Table 7 indicate that the six-phase motor has a strong potential for sustainable EV traction because it combines higher efficiency with lower thermal loading. The benefit is particularly evident during urban driving, where energy losses and temperature rise are greatest.

5.0 CONCLUSSION

Using ANSYS Motor-CAD, this study provided a comparative electrothermal assessment of three-phase and six-phase squirrel-cage induction motors for electric vehicle traction during HWFET, WLTP, and urban stop-and-go driving patterns. The impact of phase number on electromagnetic and thermal performance was carefully evaluated by maintaining the same rated power, vehicle operating conditions, traction requirements, cooling conditions, and drive-cycle inputs. The results show that, the conventional three-phase arrangement is routinely outperformed by the six-phase induction motor. The three-phase motor achieved mean efficiencies of 88.7%, 86.9%, and 82.8%, while the six-phase motor achieved mean efficiencies of 91.4%, 90.1%, and 87.3% during

HWFET, WLTP, and urban operation, respectively. Additionally, the maximum stator temperature dropped from 118.6 to 101.4°C in urban settings, from 104.7 to 93.1°C during WLTP, and from 91.8 to 82.6°C during HWFET. The corresponding cycle-integrated energy-loss reductions were roughly 16.3%, 16.5%, and 18.7%, in that order. The results also show that the six-phase topology's performance advantage increases as the driving cycle intensity increases. The biggest improvements were made in urban stop-and-go situations, where frequent acceleration and deceleration led to higher heat accumulation and current loading. Better thermal resistance is suggested by the lower rotor and winding temperatures, while increased energy efficiency is demonstrated by the reduced losses. Since motor efficiency and thermal performance have a direct impact on energy consumption, sustained power capability, and potential driving distance, these attributes are particularly advantageous for EV applications.

References

Abdelwanis, M. I. (2025). Optimizing the performance of six-phase induction motor-powered electric vehicles with fuzzy-PID and DTC. *Neural Computing and Applications, 37*, 9721–9734. https://doi.org/10.1007/s00521-024-10455-0

Ahmad, H., Dhamodharan, P., & Kim, S. C. (2025). Advances in cooling technologies for electric vehicle drive motors, reducers, and inverters. A comprehensive review. *Energy Technology*. https://doi.org/10.1002/ente.202401691

Eke, A., Okoro, O. & Onah, A.J. (2026). Design and optimization of three phase induction motor for extreme temperatures applications in oil and gas industry. *Discov Electron* **3**, 107 (2026). https://doi.org/10.1007/s44291-026-00257-0

El Baghdadi, M., & Hegazy, O. (2023). Multiphase motors and drive systems for electric vehicle powertrains: State of the art analysis and future trends. *Energies, 16*(2), 768. https://doi.org/10.3390/en16020768

Prasanna, R., Raja, S., Rusho, M. A., Sharma, S., Ramachandran, T., Arunachalam, K. P., Tejani, G. G., & Fish, H. (2026). Comparative thermal performance analysis of induction and interior permanent magnet machines for electric vehicles under varying drive cycles using ANSYS Motor-CAD software: Approach toward sustainability. *Engineering Reports, 8*(2), e70617. https://doi.org/10.1002/eng2.70617

Priyanka, C. P., Nair, N. S., & Jagdanand, G. (2022). Thermal analysis of multiphase induction motor for electric vehicle applications. In *2022 IEEE Transportation Electrification Conference & Expo (ITEC)* (pp. 801–806). IEEE. https://doi.org/10.1109/ITEC53557.2022.9813800

Selvin Raj, J. A. P., Asirvatham, L. G., Angeline, A. A., Manova, S., Rakshith, B. L., Bose, J. R., Mahian, O., & Wongwises, S. (2024). Thermal management strategies and power ratings of electric vehicle motors. *Renewable and Sustainable Energy Reviews, 189*, 113874. https://doi.org/10.1016/j.rser.2023.113874

Shewalkar, A. G., Dhoble, A. S., & Thawkar, V. P. (2024). Review on cooling techniques and analysis methods of an electric vehicle motor. *Journal of Thermal Analysis and Calorimetry, 149*, 5919–5942. https://doi.org/10.1007/s10973-024-13091-x

Tarchała, G., & Listwan, J. (2025). Space vector modulation methods with modified zero vector distribution for electrical vehicle drives with six-phase induction motor operating under direct field-oriented control. *Energies, 18*(12), 3122. https://doi.org/10.3390/en18123122

Wang, X., Li, B., Gerada, D., Huang, K., Stone, I., Worrall, S., & Yan, Y. (2022). A critical review on thermal management technologies for motors in electric cars. *Applied Thermal Engineering, 201*, 117758. https://doi.org/10.1016/j.applthermaleng.2021.117758

Zeng, X., *et al*. (2025). Power flow simulation and thermal performance analysis of electric vehicles under standard driving cycles. *Energies, 18*(14), 3737.

AVAILABILITY OF DATA AND MATERIAL: Not applicable

COMPETING INTERESTS: The authors declare that they have no competing interests related to the content of this manuscript

FUNDING: Not Applicable

DECLARATIONS

ETHICAL APPROVAL: This research did not include human subjects or animals. All data utilized were sourced from secondary sources, simulation models, and publicly accessible system parameters; hence, ethical approval was unnecessary for this study.

CONSENT TO PARTICIPATE: Consent to participate was not required.
CONSENT TO PUBLISH: Consent to publish was not required.

DATA AVAILABILITY: The datasets generated during and/or analysed during the current study are available from the corresponding author on reasonable request.

AUTHORS' CONTRIBUTIONS

1. **Asuquo Eke:** Conceptualization, Methodology, Data curation, Analysis and Writing
2. Ake David: Analysis and Writing
3. **Ohiero Peter:** Review,
4. **O. I. Okoro:** Review, Editing and Supervision
5. **A. J. Onah:** Review, Editing and Supervision
6. **E.** J. Akpama: Review, Editing and Supervision

ACKNOWLEDGEMENTS: Not Applicable